Available online at www.sciencedirect.com

ScienceDirect

Geochimica et Cosmochimica Acta 330 (2022) 116–130

Geochimica et Cosmochimica Acta

www.elsevier.com/locate/gca

High solubility of gold in H_2S-H_2O ± NaCl fluids at 100–200 MPa and 600–800 °C: A synthetic fluid inclusion study

Maokang Hu [a,b], I-Ming Chou [a,*], Ruoheng Wang [a,c], Linbo Shang [d], Chen Chen [d]

[a] *CAS Key Laboratory of Experimental Study Under Deep-sea Extreme Conditions, Institute of Deep-sea Science and Engineering, Chinese Academy of Sciences, Sanya 572000, China*

[b] *Hainan Tropical Ocean University, Sanya 572022, China*

[c] *University of Chinese Academy of Sciences, Beijing 100871, China*

[d] *State Key Laboratory of Ore Deposit Geochemistry, Institute of Geochemistry, Chinese Academy of Sciences, Guiyang 550081, China*

Received 1 July 2021; accepted in revised form 3 March 2022; Available online 9 March 2022

Abstract

Numerous previous experimental and theoretical studies of gold deposits in the Earth's crust have shown that chloride and hydrosulfide are the most abundant ligands in the relevant hydrothermal fluids. However, most of these studies were performed with solutions under relatively oxidizing conditions in the presence of SO_4^{2-}, HSO_4^-, and S_3^-. Reduced sulfur with a −2 valence (e.g., H_2S, HS^-, etc.) may play a key role in controlling redox conditions and promoting the migration of gold during the formation of epithermal and porphyry gold-copper deposits. To examine this possibility, we performed experiments in reduced H_2S-bearing fluids to constrain the effects of temperature, pressure and NaCl concentration on Au solubility through the synthetic fluid inclusion method. Measured amounts of H_2S and aqueous solutions (H_2O ± NaCl) were loaded in an Au capsule containing a fractured quartz column, and fluid inclusions were formed through healing of these fractures at specified pressures (100 or 200 MPa) and temperatures (600, 700 or 800 °C) for 20 days. Thin sections with both sides polished were prepared from quenched quartz columns, and conventional microthermometric measurements were performed. Raman spectra were collected from all phases in the fluid inclusions from room temperature to 300 °C to identify sulfur species and potential Au-bearing complexes. In all fluid inclusions, S and H_2S_n ($n \geq 1$) species were identified, but SO_2 and SO_4^{2-}, HSO_4^- and S_3^- ions were not observed. Au concentrations in these fluid inclusions, which were analyzed using LA-ICP-MS with NaCl or RbCl reference standards, ranged from 91 to 3599 ppm; they were greatly affected by pressure and NaCl concentration but not obviously by temperature. H_2S_n ($n > 1$) analogs have chemical properties similar to those of H_2S, and their deprotonation products (HS_n^- and S_n^{2-}) exhibit high affinities for Au in aqueous solution. Therefore, HS_n-Au (or AuS_n^-) and Au-Cl could be the dominant species in H_2S-bearing hydrothermal fluids and may play important roles during the dissolution and transport stages of Au in ore formation processes.

Keywords: Au solubility; H_2S-bearing hydrothermal fluid; HS_n-Au (or AuS_n^-); LA-ICP-MS; Synthetic fluid inclusion

1. INTRODUCTION

Gold is one of the most precious metals and is concentrated in hydrothermal deposits, such as porphyry gold-copper deposits, epithermal gold deposits, orogenic gold deposits and volcanogenic massive sulfide deposits. These deposits formed from fluids with reduced sulfur, as indi-

* Corresponding author.
E-mail address: imchou@idsse.ac.cn (I-Ming Chou).

https://doi.org/10.1016/j.gca.2022.03.006
0016-7037/

cated by the fact that primary ore minerals are predominantly sulfides, and reduced sulfur is thought to play an important role in the formation of gold deposits (Berndt et al., 1994; Emsbo et al, 2003; Seo et al., 2009, 2012; Pokrovski et al., 2014, 2015; Pokrovski and Dubessy, 2015). Furthermore, in the following three studies of the subduction zone sulfur cycle: (1) Li et al. (2020) suggested that sulfur recycling of typical oceanic lithosphere is dominated by reduced aqueous H_2S and HS^- in slab fluids, based on textural and thermodynamic evidence; (2) Tomkins and Evans (2015) showed that H_2S was released via pyrite breakdown well into the eclogite facies, which may coincide with slab melting or generation of supercritical liquid driven by influx of serpentinite-derived fluids; and (3) Jégo and Dasgupta (2013) showed that under their experimental conditions, which involved a synthetic H_2O-saturated MORB (mid-ocean ridge basalt), 1 wt.% S (added as pyrite) as a starting material, pressures (P) of 2.0 and 3.0 GPa, temperatures (T) ranging from 800 to 1050 °C, and the use of either Ni–NiO (NNO) or Co–CoO (CCO) as an external oxygen fugacity (fO_2) buffer, the hydrous fluid phase was mainly composed of H_2S and H_2O. Therefore, knowledge of the dominant Au species and Au solubility in hydrothermal fluids containing reduced sulfur, such as H_2S, at high Ts and Ps is essential for our understanding of the mechanism for formation of Au deposits.

Gold in hydrothermal fluids has been suggested to form complexes with HS^-, S^{2-}, Cl^- and other ligands. For example, based on measurements of gold solubility in aqueous sulfide solutions at the pyrite-pyrrhotite redox buffer, between 100 and 300 °C, Seward (1973) deduced that the dominant Au species in acidic, neutral and alkaline solutions are $AuHS^0$, $Au(HS)_2^-$ and $Au_2(HS)_2S^{2-}$, respectively. This conclusion relating gold species in hydrothermal fluids with reduced sulfur was supported by most of the experiments run below 500 °C (Hayashi and Ohmoto, 1991; Benning and Seward, 1996; Gibert et al., 1998; Dadze et al., 2000; Stefánsson and Seward, 2004; Tagirov et al., 2005; Pokrovski et al., 2009b). In addition, polysulfide ions (S_n^{2-} and HS_n^-) have been shown to form strong complexes with Au in aqueous solution (Berndt et al., 1994; Tossell et al., 1996; Pope et al., 2005; Pokrovski et al., 2009b; Pokrovski and Dubrovinsky, 2011; Liu et al., 2013), and S_3^- ions, as other polysulfide ions, exhibit a high affinity for chalcophilic metals (Pokrovski and Dubrovinsky, 2011; Pokrovski et al., 2014, 2015; Pokrovski and Dubessy, 2015; Colin et al., 2020). Pokrovski et al. (2015) showed that the amount of $Au(HS)S_3^-$ complex increased with increasing S_3^- ion in certain geologically relevant T-P-pH-fO_2 conditions, and it became a dominant Au-bearing species in hydrothermal solutions above 300 °C. In addition, gold chloride has been suggested as the dominant species present under oxidizing conditions in salt-rich fluid lacking reduced sulfur and strong acid (Gammons and Williams-Jones, 1997; Pan and wood, 1991; Stefánsson and Seward, 2003; Pokrovski et al., 2009a; Guo et al., 2018). Based on first-principles molecular dynamics calculations on the hydration and acidity of polysulfide species, Liu et al. (2013) predicted that H_2S_n, HS_n^- and S_n^{2-} can all be dominant at common pH levels (3–9) and that Au^+-HS_n^- complexes can form in solutions such that polysulfides can act as metal complexing agents in hydrothermal processes. HS_n^- and S_n^{2-} have chain-like molecular structures and form complexes with many transition metal cations (e.g., Fe^{2+}, Cu^{2+}, Zn^{2+}), and the high concentrations of gold in some springs in New Zealand were attributed to polysulfide complexes (Pope et al., 2005).

Not only are the complexes of gold controversial, but the solubility of gold varies greatly in hydrothermal experiments. The content of gold in natural fluid inclusions from several porphyry Cu-Au deposits is approximately 1 ppm (Heinrich et al., 1999; Ulrich et al., 2002; Williams-Jones and Heinrich, 2005; Landtwing et al., 2010; Seo et al., 2009, 2012), but Au solubility in hydrothermal experiments could be up to 1180 ppm in iron sulfide-saturated brines (Loucks and Mavrogenes, 1999). Most experimental studies of Au complexes, their solubilities, and the factors influencing gold solubility in hydrothermal sulfide-bearing solutions have been performed at temperatures below 500 °C (Hayashi and Ohmoto, 1991; Benning and Seward, 1996; Stefánsson and Seward, 2004; Tagirov et al., 2005), and the characteristics of gold in hydrothermal fluids at higher Ts cannot be deduced from these experimental results. Therefore, the main purposes of this study were (1) to determine the solubility of Au in H_2S-bearing hydrothermal fluids at 100–200 MPa and 600–800 °C; (2) to detect or deduce the presence of potential Au complexes; (3) to examine the effects of T, P and NaCl concentration on gold solubility in hydrothermal fluids; and (4) to determine whether HS_n-Au (or AuS_n^-) and Au-Cl species are present in H_2S-bearing hydrothermal fluids and whether they play a role during the dissolution and transport of Au in ore formation processes. Our experiments were conducted by (1) synthesizing fluid inclusions (FIs) in quartz in Au capsules at 100–200 MPa and 600–800 °C with starting fluids of known compositions containing H_2O-H_2S ± NaCl; (2) analyzing the synthetic FIs with microthermometric and Raman spectroscopic methods; and (3) using the LA-ICP-MS method to determine the amounts of dissolved Au in FIs.

2. MATERIALS AND METHODS

Syntheses of fluid inclusions and related microthermometric and Raman spectroscopic studies were performed in the CAS Key Laboratory of Experimental Study under Deep-sea Extreme Conditions, Institute of Deep-sea Science and Engineering, Chinese Academy of Sciences (CAS), while LA-ICP-MS analyses of Au concentration in the fluid inclusions were performed in the State Key Laboratory of Ore Deposits Geochemistry, Institute of Geochemistry, CAS.

2.1. Fused-silica capillary capsule for quantitative H_2S loading

To load H_2S quantitatively in an Au capsule for synthesizing FIs, a fused silica capillary capsule (FSCC, OD = 1.00 mm, ID = 0.83 mm, length = ~2 cm) containing H_2S was prepared by sealing both ends of the fused-silica capillary (Polymicro Technologies, LLC) with a hydrogen

flame. The H_2S-loading system (Fig. 1; Chou et al., 2008) consisted of corrosion-resistant *P* valves and stainless steel tubes (High Pressure Equipment Co.), a *P* gauge (Omega, DPG4000), a vacuum pump (Ultimate vacuum = 10 Pa), and a fluid tank of H_2S (99.99%, Messer Group). After one end of the silica tube was sealed with a hydrogen flame, the other (open) end of the tube was connected to a *P* line, then evacuated and flushed with gaseous H_2S three times before loading H_2S. When the *P* of the loaded H_2S was adjusted to approximately 2 bar, the closed end of the capillary tube was immersed in liquid nitrogen to precipitate H_2S, and the open end of the capillary tube was sealed under vacuum with a hydrogen flame to obtain an FSCC containing both pure vapor (V) and liquid (L) H_2S (Fig. 1). The mass of H_2S in each FSCC with 0.83 mm ID was then determined by measuring the lengths of the L and V phases of H_2S under a microscope to obtain the volumes of these phases, which were then converted to their masses based on their room *T* densities (Table 1).

2.2. Synthetic fluid inclusion

FI-free Brazilian quartz was used as the host of the fluid inclusion, and a homogeneous fluid was captured and formed FIs through healing of fractures in quartz (Sterner and Bodnar, 1984; Loucks and Mavrogenes, 1999; Duc-Tin et al., 2007; Zhang et al., 2012; Guo et al., 2018). Quartz columns (approximately 2 mm × 2 mm × 15 mm) were heated to 350 °C and quenched in deionized water to produce a large number of cracks and then dried at 110 °C for 12 hours. A fixed amount (15 μl) of NaCl aqueous solution or deionized water, together with a fractured quartz column and an H_2S-bearing FSCC, were loaded into a gold tube (OD = 4.4 mm, ID = 4.0 mm, length = ~3 cm), which had been cleaned and sealed at one end. The open end of the gold tube was then connected to a vacuum line before using a pinch-off device to cut and cold weld the gold capsule under vacuum and eventually sealed it through argon arc welding. Six Au capsules were prepared accordingly for six individual experiments (Table 1), and the loaded NaCl solutions in four Au capsules contained dilute RbCl (400 ppm) and CsCl (300 ppm), which were added to provide references for quantitative LA-ICP-MS analyses of Au.

A loaded gold capsule was placed in a rapid-quench cold-sealed pressure vessel made of Inconel 713LC superalloy (CSPV; Matthews et al., 2003; Guo et al., 2018) and heated for 20 days at a fixed *T* between 600 and 800 °C after being pressurized with H_2O at a fixed *P* of either 100 or 200 MPa. Sample *T* was measured by a K-type thermocouple inserted in a well of the CSPV near the sample, and the reported *T* was accurate to within ± 5 °C at 800 °C. Sample *P* was measured by a precalibrated gauge with an uncertainty of less than 5%. The redox state of the sample under a fixed *P-T* condition was not rigorously controlled, but it should be more reducing than that of the *P* medium in the CSPV, which is believed to be near that of the Ni-NiO buffer because the CSPV is Ni-rich (76 wt% Ni) (Guo et al., 2018). Because the Au capsule had limited permeability to hydrogen (Chou, 1986) under the experimental *P-T* conditions and was initially loaded with H_2S, the redox state of the sample in the Au capsule should be more reducing than that of the external *P* medium. During the process of pressurization and heating, the FSCC enclosed in the gold capsule was crushed, and it released H_2S before reaching the experimental *P-T* condition. After cooling to room temperature, the quartz column was cleaned and then cut into approximately 1 mm thick chips, which were then polished on both sides and examined on a Linkam CAP500 freezing/heating stage under a microscope. The FI *T*s were controlled to within ± 0.2 °C during microthermometric analyses and collection of Raman spectra.

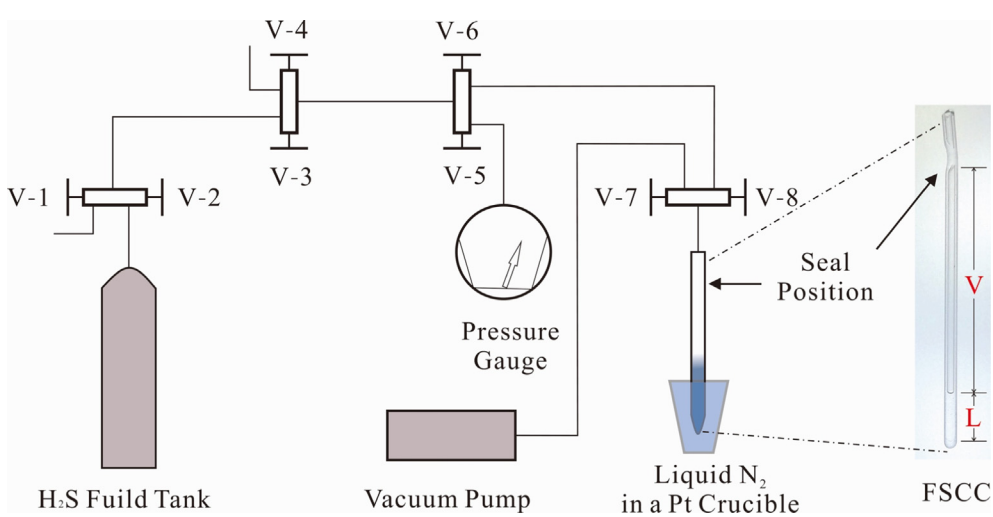

Fig. 1. Schematic diagram of H_2S loading system. The photo on the right side shows vapor (V) and liquid (L) H_2S phases in a fused-silica capillary capsule sealed at both ends (FSCC; OD = 1.00 mm, ID = 0.83 mm, length = ~2 cm), which was constructed following the procedures of Chou et al. (2008). V-1 to V-8 are three-way/two-stem combination taper-seal valves (HIP 15-15AF1), which were connected with high-pressure stainless-steel tubes.

Table 1
Experimental conditions and results.

Exp. #	*T* (℃)	*P* (MPa)	H_2S in FSCC[a] (mg)	Loaded aqueous solution (15 μl)				H_2S/H_2O Mass ratio[c]	Measured Rb/Cs Mass ratio[d]	Measured ^{197}Au (ppm)[e]			
				H_2O[b] (mg)	NaCl (wt%)	RbCl (ppm)	CsCl (ppm)			^{23}Na Std.	Ave. (Stdev.)	^{85}Rb Std.	Ave. (Stdev.)
1	600	200	3.34	15.00	-	-	-	0.22	-	-		-	
2	600	200	4.62	14.91	1%	-	-	0.31	-	923	1161	-	-
										1726	(449)		
										702			
										1293			
3	700	200	4.63	14.91	1%	400	300	0.31	1.24	1398	1311	1500	1517
									1.11	1271	(71)	1348	(304)
									0.97	1338		1950	
									1.20	1238		1270	
4	800	200	4.70	14.91	1%	400	300	0.32	1.11	984	897	947	941
									1.36	831	(108)	745	(206)
									1.03	831		911	
									1.11	799		819	
									1.08	1041		1283	
5	600	100	4.73	14.91	1%	400	300	0.32	1.20	213	282	192	199
									1.27	-	(179)	91	(114)
									1.25	485		357	
									1.35	147		154	
6	600	200	4.80	14.43	10%	400	300	0.33	1.15	3338	3074	3599	3272
									1.27	2730	(312)	2659	(532)
									1.20	3155		3559	

[a] Calculated from the volumes of liquid and vapor phases loaded in FSCC and their densities at room *T*.
[b] Calculated from the densities of 1 wt% or 10 wt% NaCl aqueous solutions (Mao and Duan, 2008).
[c] Initial mass ratio loaded into an Au capsule.
[d] All measured values are within the error range (±0.22) of the loaded value of 1.19.
[e] Based on either ^{23}Na or ^{85}Rb internal standard. Additionally, average values (Ave.) and standard deviations (Stdev.) are listed for each experiment.

2.3. LA-ICP-MS analyses and Raman spectra collection

The LA-ICP-MS consists of an Agilent 7900 ICP-MS and a GeoLasPro 193 nm ArF laser. The sample compartment was a standard stripping cell, in which a mold made of resin was added to provide a smaller volume of sampling space. During this process, memory effects and the wash time of the cell were reduced. Helium was used as the carrier gas, which was mixed with argon via a T-connector before entering the ICP-MS instrument. To enhance the intensities of ICP-MS signals, 3 ml/min nitrogen was also added to the mass spectrometer. Laser energy of 10 Hz and 11 J/cm^2 was selected for the analyses. Laser spot sizes of 24–44 μm were used, depending on the size and depth of the inclusion in quartz. Masses of ^{23}Na, ^{29}Si, ^{35}Cl, ^{85}Rb, ^{133}Cs and ^{32}S were analyzed with a dwell time of 20 ms, but a dwell time of 50 ms was selected for ^{197}Au. The external standard was based on NIST SRM 610 (Jochum et al., 2011). The internal standard was based on the Na concentration of the loaded solution or the Rb and Cs concentrations in the starting fluid. Host correction was applied during data processing. The data collected from ICP-MS were calibrated, background corrected, and integrated signal floating processed using the software Sills (Guillong et al., 2008).

Raman spectra were obtained with a JY/Horiba LabRam HR Evolution Raman spectrometer using a 532.06 nm (Nd:YAG) laser with an initial power of 100 mw, an SLWD 50x Olympus objective with 0.35 numerical aperture, and a grating with 1800 grooves/mm and a spectral resolution of approximately 0.2 cm^{-1}. Wavelength calibration was accomplished with Ne emission lines (2516.343 and 2710.673 cm^{-1}) and the principal vibrational band of silicon (520.7 cm^{-1}). PeakFit v. 4.0 (AISN Software Inc.) was used to calculate the characteristic peak positions of the spectra collected.

3. RESULTS

3.1. Appearance of fluid inclusions and observed phase relations

Although the initial compositions and *P-T* conditions of the six experiments listed in Table 1 were not identical, all synthesized FIs, except those from Exp. #1 contained three phases at room *T*, vapor (V), liquid (L_{H2O}) and solid (S) phases; all of which had irregular or nearly elliptical shapes with sizes ranging between 5 and 30 microns (Fig. 2). Raman spectroscopic analyses of these phases showed that the vapor phase was dominated by H_2S, the liquid phase by H_2O with dissolved H_2S, and the solid phase by sulfur, a daughter mineral not present at higher *T*s (Fig. 3). The diameters of the solid phases were generally less than 2 microns, and increased with increasing volume of inclusion. These three coexisting phases in FIs from the same experiment observed at room *T* have similar volume ratios, indicating that a homogeneous fluid was trapped in these FIs (Frezzotti et al. 2012).

The starting fluid in Exp. #1 contained higher H_2S levels than other samples, and the synthetic FIs had an additional phase, liquid H_2S, which exhibited minor abundance and was difficult to observe at room *T* but was clearly identified by Raman analysis around the S phase. When these FIs were frozen and then heated to 23 °C, hydrogen sulfide hydrate (H), aqueous solution (L_{H2O}), and hydrogen sulfide gas (V) coexisted (Fig. 3). During heating, the hydrogen sulfide hydrate dissolved at 26 °C. As shown in Fig. 3, when these FIs were heated to 250 °C, little change was observed in the size of the S phase, but it disappeared at 300 °C before total homogenization of the FI at 326 °C. On the other hand, the S phases in the FIs from Exps. #2∼#6 were still present after homogenization of the vapor and liquid phases at 328, 374, 382, 365 and 385 °C, respectively. To prevent the loss of FI samples from decrepitation, attempts were not made to measure the disappearance *T*s of the S phase in these FIs, but they should be well below *T*s at which the FIs were synthesized.

3.2. Raman spectra of phases in fluid inclusions

Fig. 4A shows Raman spectra of H_2S vapor (H_2S_V; ∼2610 cm^{-1}), H_2S hydrate (H_2S_H; ∼2593 and ∼ 2603 cm^{-1}) and dissolved H_2S in H_2O (H_2S_{aq}; ∼2593 cm^{-1}) collected froman FI synthesized in Exp. # 1 at room *T* (23 °C) and, for comparison, the spectrum of liquid H_2S (H_2S_L; ∼2581 cm^{-1}) collected from an FSCC. Fig. 4B shows a Raman spectrum collected from the solid phase (S) in an FI synthesized in Exp. # 2, with two peaks near 2497 and 2568 cm^{-1}; the presence of these two bands in the spectra of S-H_2S systems is a common phenomenon, and they were assigned to the S-H stretching vibrations of H_2S_n and H_2S in S, respectively (Wiewiorowski and Touro, 1966; Tritlla et al., 2000; Hurai et al., 2019). In Fig. 4C, a Raman spectrum collected from the S phase in an FI synthesized in Exp. # 1 shows an additional band at ∼ 2581 cm^{-1}, which is probably derived from a small amount of liquid H_2S around the S.

The Raman spectrum of the aqueous phase collected at 100 °C from an FI in quartz synthesized in Exp. #2 is compared with that collected at 300 °C in Fig. 5. Most of the Raman bands shown in Fig. 5A and 5B were derived from the host quartz (all marked bands; https://rruff.info/), and those shown in Fig. 5C were from H_2O (3000–3700 cm^{-1}) and dissolved H_2S (∼2590 cm^{-1}). It is important to point out that no signals shown in Fig. 5 indicate the presence of SO_4^{2-} (∼980 cm^{-1}; Frezzotti et al., 2012; Wang et al., 2013;), HSO_4^- (∼1050 cm^{-1}; Dubessy et al., 1992; Wang et al. 2013; Schmidt and Seward, 2017) or S_3^- (∼534 cm^{-1}; Pokrovski and Dubrovinsky, 2011; Schmidt and Seward, 2017; Colin et al. 2020).

The solid daughter phase (S) in all FIs was identified as sulfur by the presence of α-sulfur Raman bands at 150 ± 1, 220 ± 1, and 474 ± 1 cm^{-1} (Frezzotti et al. 2012; Jacquemet et al. 2014) (Fig. 6). In addition to the fingerprint region of these diagnostic α-sulfur bands, Raman spectra of sulfur grains in all inclusions included S-H stretching vibration bands at 2497 ± 1 and 2568 ± 1 cm^{-1} (Fig. 4B and 4C).

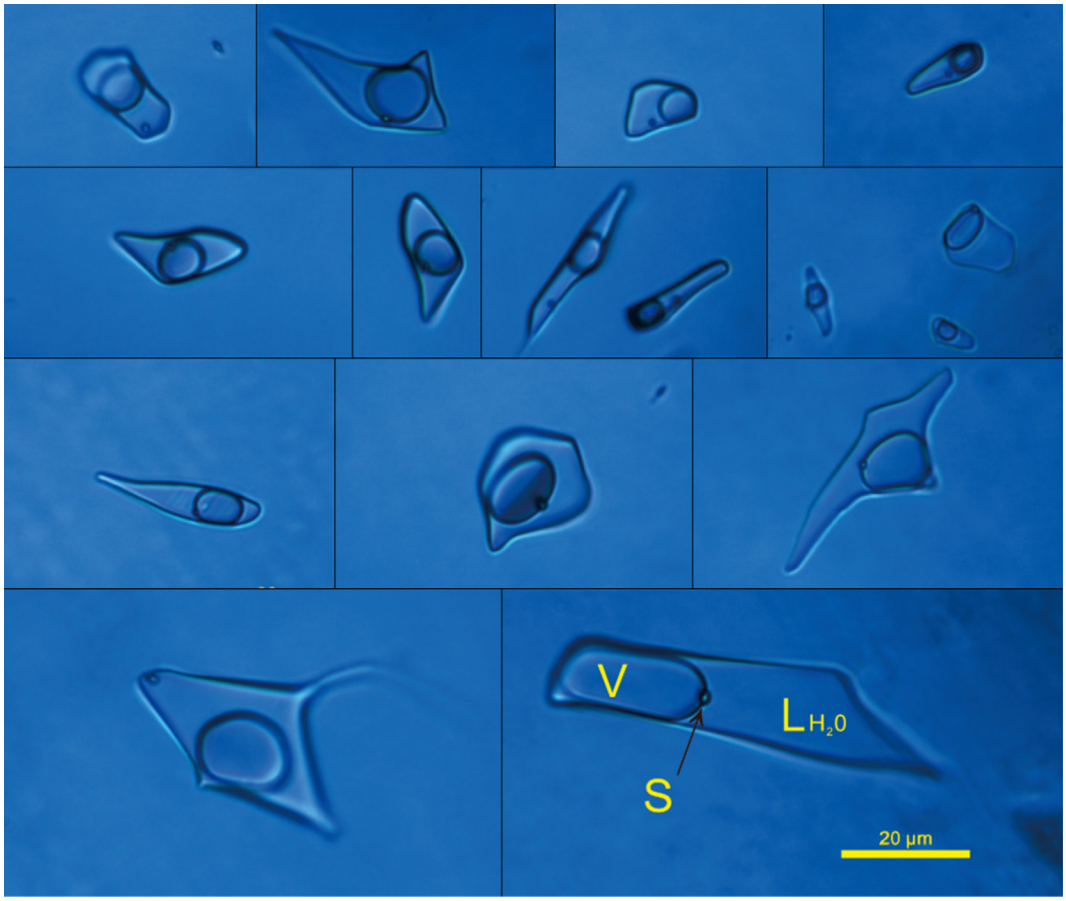

Fig. 2. Photomicrographs of FIs in quartz synthesized at 600 °C and 200 MPa in a gold capsule for 20 days (Exp. # 2). All inclusions contained a vapor phase (V; dominated by H_2S), an aqueous phase (LH_2O; with dissolved H_2S) and a daughter phase (S; identified as sulfur particles containing H_2S and H_2S_n). Note that all FIs have similar volume ratios among the three coexisting phases.

3.3. Au solubility based on LA-ICP-MS analyses of synthetic fluid inclusions and the effects of *T*, *P* and Cl^- concentrations on Au solubility

Representative LA-ICP-MS signals from an FI analysis are shown in Fig. 7, and the results for all analyses are listed in Table 1. The average solubility of gold in Exps. #2 to #6 were 1161, 1311, 897, 282 and 3074 ppm, respectively, and they were calculated by using sodium chloride as an internal standard; similar solubilities were obtained by using rubidium chloride as the standard (Table 1). Previous studies showed that the solubility of Au in hydrothermal fluid is affected by *T*, *P*, pH, oxygen fugacity (fO_2) and ligand (S or Cl) concentration (Seward, 1973; Hayashi and Ohmoto, 1991; Loucks and Mavrogenes, 1999; Stefánsson and Seward, 2004; Pokrovski et al., 2009b; Guo et al., 2018). To determine the effects of *T*, *P* and Cl^- concentration on Au solubility in this study, pH values were limited to solutions saturated with hydrogen sulfide (pH ~ 4.1), hydrogen sulfide contents were approximately 4.7 ± 0.1 mg in 15 μl volumes of these solutions, and fO_2 was controlled by the starting materials. Despite the long durations (20 days) of FI syntheses in all experiments, fO_2 in the FIs remained below the S-H_2S equilibrium condition because S identified at low *T*s may not exist at experimental *T*s. As shown in Fig. 8, the solubility of gold increased first and then decreased as *T* increased from 600 to 800 °C (Fig. 8A), increased as *P* increased from 100 to 200 MPa (Fig. 8B), and increased with increasing sodium chloride concentration (1–10 wt.%; Fig. 8C). Note that, in the preliminary experiment (Exp. #1), no internal standard was included in the sample; therefore, quantitative Au solubility could not be determined, even though LA-ICP-MS signals for FI analyses (Fig. 7A without reference signals) were similar to those shown in Fig. 7B and 7C, indicating the presence of dissolved gold.

4. DISCUSSION

4.1. H_2S_n(n > 1) in reduced H_2S-S fluids and potential Au-HS_n species

Hydrogen sulfide and elemental sulfur often coexist in fluid inclusions trapped in minerals (Giuliani et al., 2003; Aguilera et al., 2016; Feneyrol et al., 2017; Hurai et al., 2019). However, polysulfanes (H_2S_n, n > 1; also named polysulfides) are rarely reported in fluid inclusions because they are thermodynamically metastable at near-surface

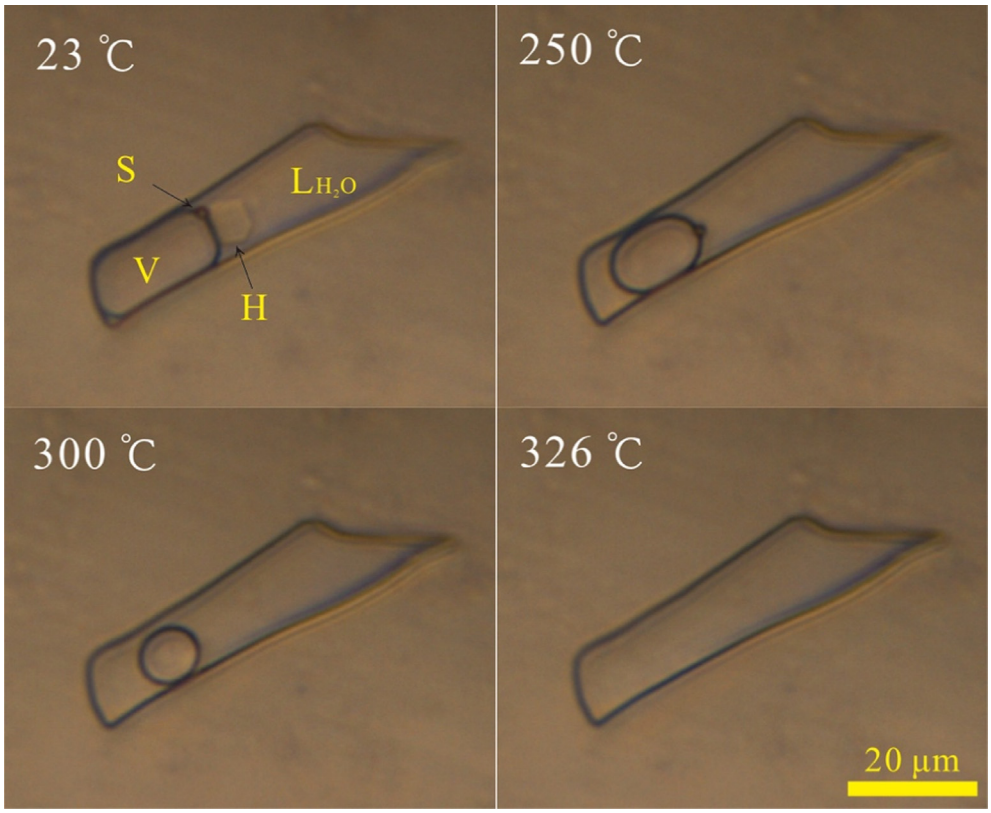

Fig. 3. Photomicrographs of an FI in quartz from Exp. #1 at various *T*s. H is hydrogen sulfide hydrate, which dissolved at 26 °C. V, S and L_{H2O} are vapor, sulfur particles, and aqueous solutions containing dissolved H_2S, respectively. The S phase dissolved at 300 °C, and total homogenization occurred at 326 °C.

conditions and are easily decomposed to elemental sulfur and hydrogen sulfide by the proposed reaction (Steudel and Eckert, 2003; Yu et al., 2021):.

$$H_2S_n \rightarrow [(n-1)/8]S_8 + H_2S \quad (1)$$

In our experiments, starting fluids contained only H_2S and H_2O, but S and H_2S_n were detected in the synthetic FIs by Raman spectroscopy near room *T*, indicating the loss of H_2 from the Au capsules during experiments. No redox control was attempted in our experiments, and apparently, the H_2 pressures produced through the reactions.

$$nH_2S \rightleftharpoons H_2S_n + (n-1)H_2 \quad (2)$$

or.

$$H_2S \rightleftharpoons S + H_2 \quad (3)$$

in the Au capsules were higher than those in the external pressure medium (H_2O) in CSPV, resulting in H_2 loss from samples via diffusion through the walls of the Au capsule. Polysulfanes are expected to exist in reduced H_2S-S fluids at high *P*-*T* conditions, according to reaction (2) or.

$$H_2S + (n-1)S \rightleftharpoons H_2S_n \quad (4)$$

and they are even being considered, together with their deprotonated products (HS_n^- and S_n^{2-}), as the dominant species of sulfur in hydrothermal fluids deep in the Earth (Migdisov et al., 1998; Steudel and Eckert, 2003; Yu et al. 2021).

Based on strong correlations between gold solubility and the abundances of aqueous polysulfide species, Berndt et al. (1994) suggested that Au-polysulfides (AuS_nS^-, n = 2–7) are the dominant Au-bearing complexes in sulfur-saturated solutions. Pokrovski and Dubrovinsky (2011) also agreed that polysulfide ions (S_n^{2-}, n > 1) exhibit a high affinity for Au and Cu, indicating a strong potential to form complexes with Au in aqueous solution. XANES spectra and quantum-chemical calculations also implied the formation of species composed of linear S-Au-S moieties (Pokrovski et al., 2009b). The dangling sulfur in HS_n^- anions has chemical properties very similar to those of HS^-, which is one of the most important metal complexing agents in ore-forming fluids. Therefore, HS_n^- analogs should also play important roles in transporting chalcophilic metal elements during hydrothermal ore-forming processes (Liu et al., 2013).

The concentration of polysulfanes in natural hydrothermal fluids were too low to be detected, and the high concentration of sulfur promoting polymerization reactions in our experiments helped us to detect polysulfanes by Raman spectroscopy. However, it should be noted that the sulfur concentrations in our experimental fluids were much higher than most magmatic and hydrothermal fluids, which may result in fluid inclusions form Au deposits contain signifi-

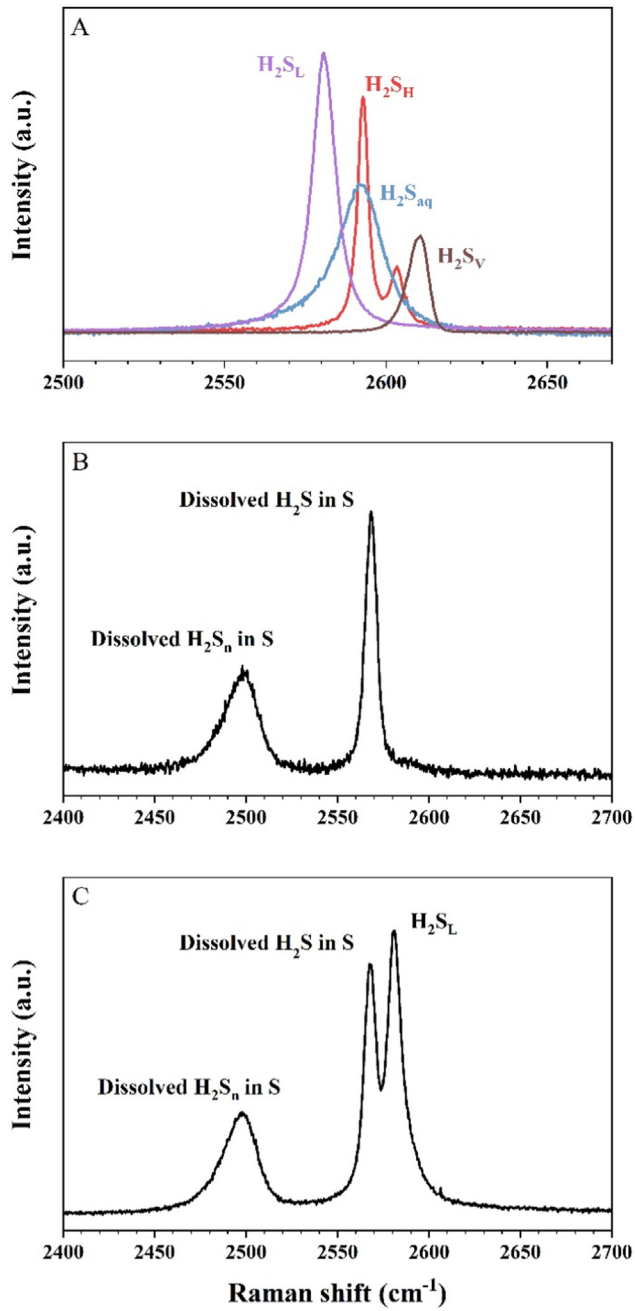

Fig. 4. (A) Raman spectra of H_2S vapor (H_2S_V), H_2S hydrate (H_2S_H) and dissolved H_2S in H_2O (H_2S_{aq}), collected from an FI in Exp. # 1, and the spectrum of liquid H_2S (H_2S_L) collected from an FSCC. (B) Raman spectrum collected from sulfur particles in an FI synthesized in Exp. # 2, showing a band at $\sim$ 2497 cm^{-1} (dissolved H_2S_n in S) and a band at $\sim$ 2568 cm^{-1} (dissolved H_2S in S). (C) Raman spectrum collected from sulfur particles in an FI synthesized in Exp. # 1, showing an additional band for liquid H_2S at $\sim$ 2581 cm^{-1}. All spectra were collected at room *T*.

cantly less Au than fluids that were synthesized experimentally.

4.2. Comparison of Au solubility in hydrothermal fluids

Heinrich et al. (1999) analyzed quartz FIs of ore-forming porphyry and granite by LA-ICP-MS, and their results showed that the Au contents in the vapor and liquid phases of the inclusions were 0.1–10 ppm and 0.1–1 ppm, respectively. The gold contents of fluid inclusions in most porphyry copper–gold deposits are generally between 0.2 and 1.3 ppm (Ulrich et al., 2002; Williams-Jones and Heinrich, 2005; Landtwing et al., 2010; Seo et al., 2009, 2012). However, the results of simulation experiments for hydrothermal fluids containing reduced sulfur showed that the solubility of gold is generally as high as tens to thou-

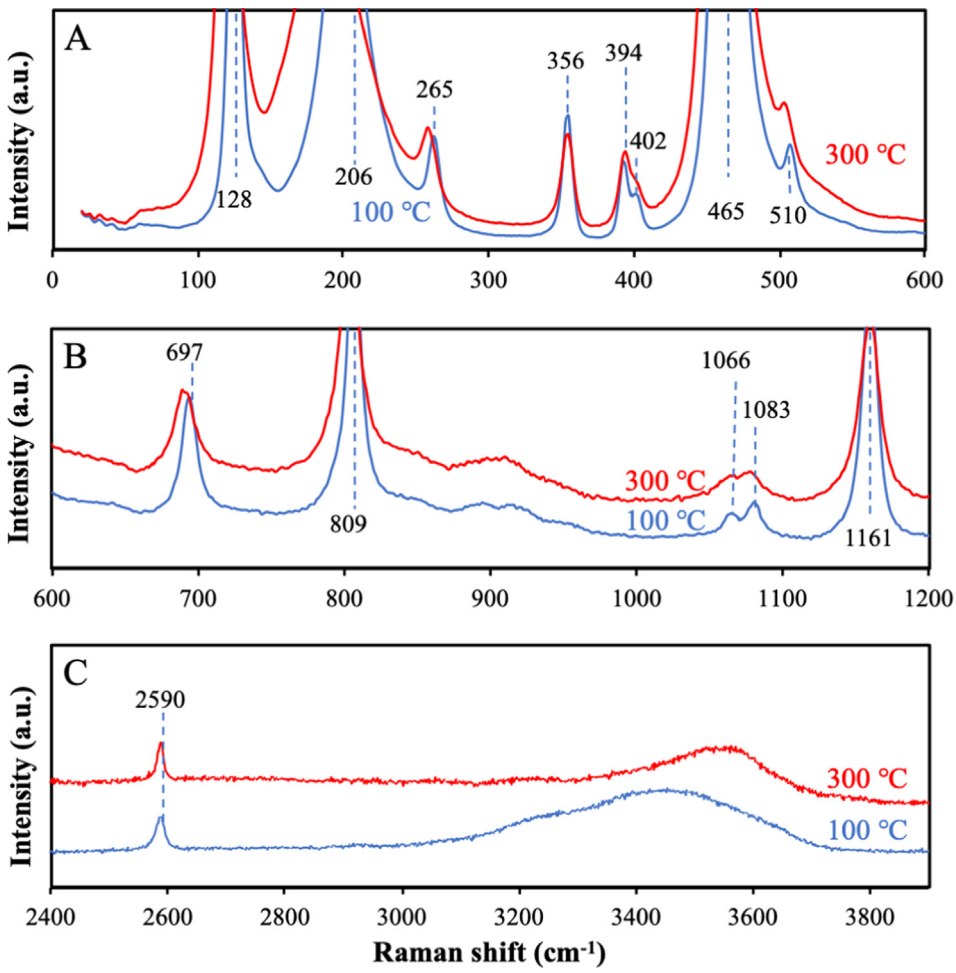

Fig. 5. Raman spectra of the aqueous phase collected at 100 and 300 °C from an FI in quartz synthesized in Exp. #2. (A) and (B) show Raman signals for quartz (marked) and background, and (C) shows Raman signals for dissolved H_2S (H_2S_{aq}) near 2590 cm^{-1} and for water (3000 ~ 3800 cm^{-1}). Note that S_3^-, HSO_4^- and SO_4^{2-} species were not detected; their Raman shifts are near 534, 980, and 1050 cm^{-1}, respectively.

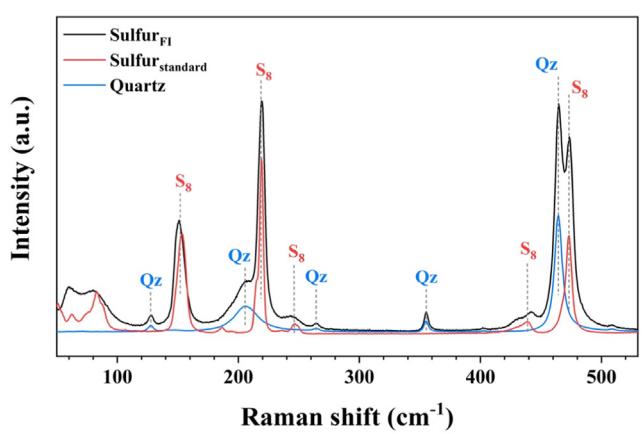

Fig. 6. Raman spectrum of sulfur particles collected at room *T* from an FI synthesized in Exp. #2.

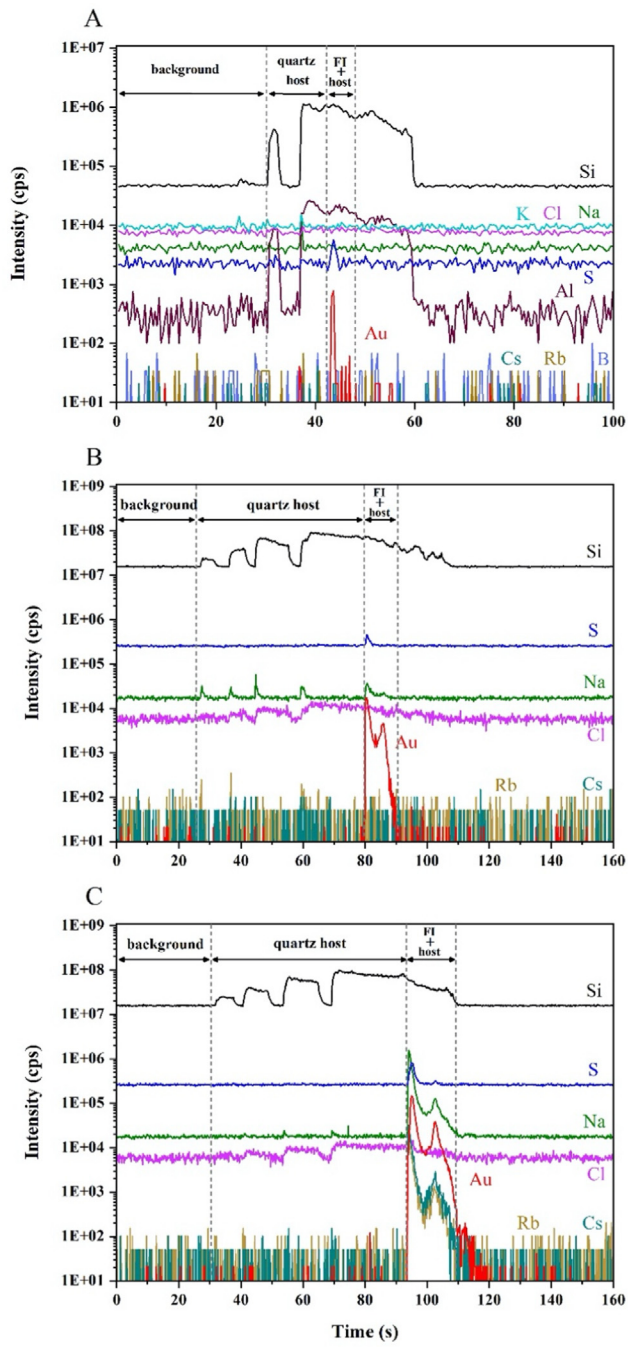

Fig. 7. LA-ICP-MS signals of elements derived from FIs synthesized in (A) Exp. #1, loaded without internal standard, (B) Exp. #2, loaded with Na standard, and (C) Exp. #6, loaded with Na, Rb and Cs standards (see Table 1). The signals for Au, Cs and Rb are shown as red, light green and brown lines, respectively.

sands of ppm (Seward, 1973; Hayashi and Ohmoto, 1991; Benning and Seward, 1996; Gibert et al., 1998; Loucks and Mavrogenes, 1999; Stefánsson and Seward, 2004; Zajacz et al., 2010, 2017).

Hayashi and Ohmoto (1991) that gold contents in typical ore-forming fluids should be within the range 0.1 ppb −1 ppm at 250–350 °C, but the gold solubility of the S + Au + NaCl + Na_2SO_4 equilibrium aqueous solution system was 0.1–66 ppm. Stefánsson and Seward (2004) performed measurements of gold solubility in an aqueous solution (Au + H_2S + H_2 + NaCl) at 100–500 °C and 500 bar using a flow-through autoclave system, and they found that the solubility range was 0.007–131 ppm. Loucks and Mavrogenes (1999) measured the gold content of chlorine-rich hydrothermal fluids by using LA-ICP-MS with synthetic FIs and found that Au solubilities of H_2S-containing FIs synthesized at 550–700 °C and 110–400 MPa were as high as 1180 ppm. Zajacz et al. (2010)

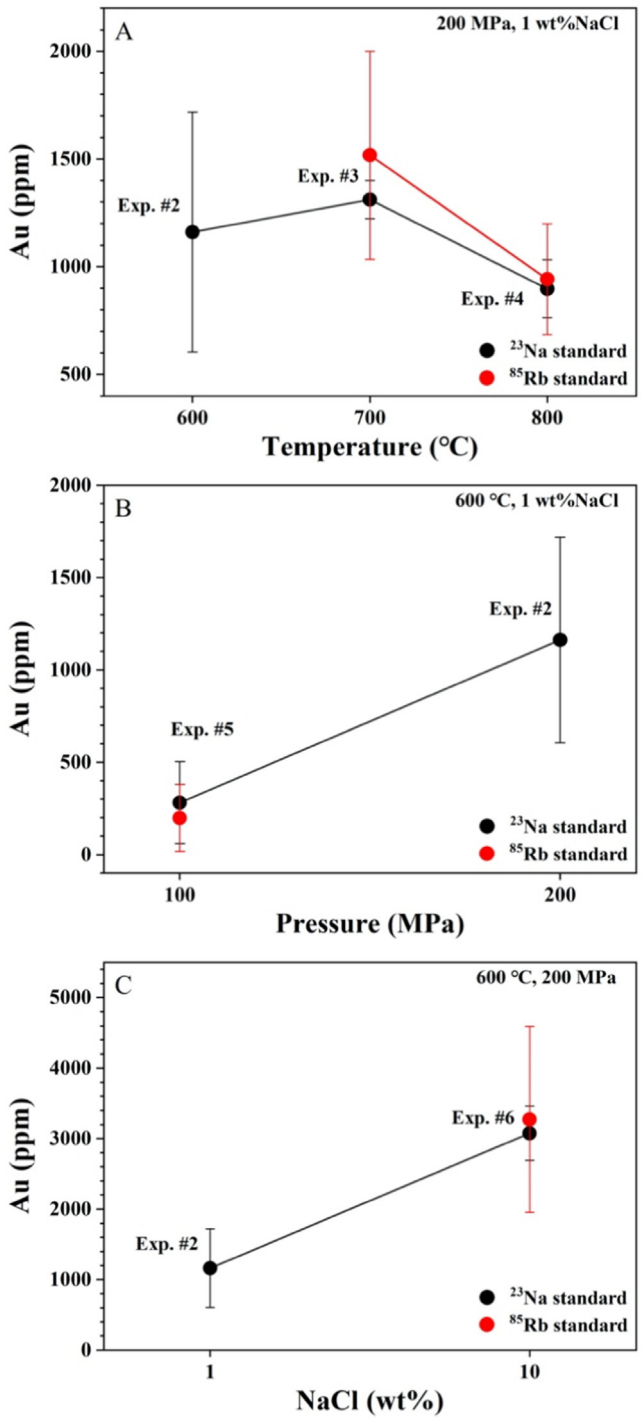

Fig. 8. Measured concentrations of gold in fluid inclusions in quartz synthesized in experiments #2 ~ 6, using sodium chloride (black) and RbCl (red) as internal standards in LA-ICP-MS analyses. The effects of *T*, *P* and NaCl concentration are illustrated in A, B and C, respectively. The dot and the vertical line represent the average and the 95% confidence interval for Au concentrations in each experiment, respectively. Plotted are the data listed in Table 1.

reported the Au solubility of up to 1500 ppm in low-density vapor-like volatile phases at 1000 °C and 150 MPa. Guo et al. (2018) systematically studied gold solubilities of hydrothermal fluids by using the synthetic FI method, and found that fluids with geologically realistic HCl contents (~1.1 wt%) and salinities (7–50 wt% $NaCl_{equiv.}$) dissolved ~ 1000–3000 ppm Au at 600 °C and 100 MPa, with oxygen fugacities controlled by magnetite-hematite buffer. In our experiments, Au solubilities in H_2S hydrothermal fluids without the addition of unreasonable

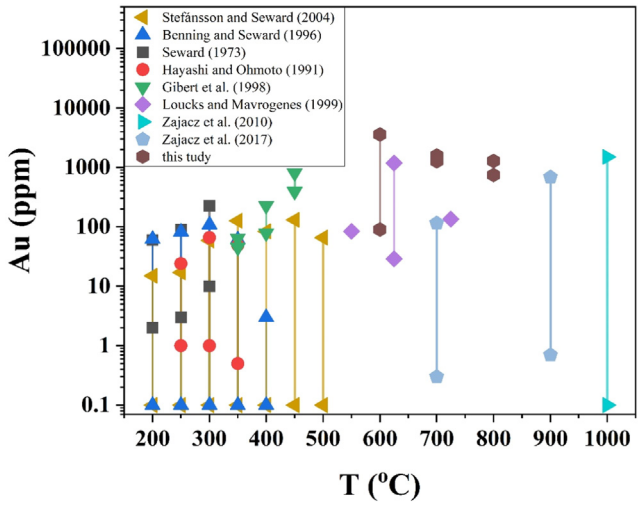

Fig. 9. Comparison of Au solubilities in representative hydrothermal experiments as a function of *T*. The effects of chemical system, in which the complexes are produced, on the solubility of gold are not considered here, nor the effects of experimental conditions, including the concentrations of H_2S and Cl^-, fO_2, *P* and pH. Note that the data of Guo et al. (2018) are not plotted here because their solutions contained geologically unrealistic concentrations of HCl and/or H_2SO_4 (e.g., 3.5 wt% HCl ± 16.4 wt% H_2SO_4), and that our measured Au solubilities are much higher than most of previously reported values.

amounts of HCl and/or H_2SO_4 (e.g., 3.5 wt% HCl ± 16.4 wt% H_2SO_4 in Guo et al., 2018) were as high as about 3600 ppm. Fig. 9, shows that our measured Au solubilities are much higher than most of previously reported values without considering the difference in experimental conditions other than *T*.

Previous studies showed that the solubility of gold is not only related to the chemical system in which the complexes are produced but also to slight changes in experimental conditions, including the concentrations of H_2S and Cl^-, fO_2, *T*, *P* and pH. For example, Seward (1973) used Au ± NaHS ± HCl ± NaCl aqueous solution as initial reactants for measuring gold solubility in a hydrothermal fluid, and the results showed that an increase in *T* or a decrease in pH significantly increased the solubility of gold. It is believed that the solubility of gold decreased as *T* decreased from 500 to 100 °C (Seward, 1973; Shenberger and Barnes, 1989; Stefánsson and Seward, 2004; Williams-Jones et al., 2009). Hayashi and Ohmoto (1991) showed that an increase in pH leads to the precipitation of gold, especially for hydrothermal fluids containing $Au(HS)_2^-$. When the pH of the hydrothermal fluid is acidic, increasing the pressure also increases the solubility of gold above 150 °C (Benning and Seward, 1996). We did not take pH as a variable in our experiments. An increase in fO_2 increases the solubility of gold, whether gold exists in the form of Au-S or Au-Cl (Shenberger and Barnes, 1989; Hayashi and Ohmoto, 1991; Guo et al., 2018). In hydrothermal fluids containing hydrogen sulfide and sodium chloride, gold solubility increases with increasing H_2S activity (Hayashi and Ohmoto, 1991; Benning and Seward, 1996; Zajacz et al., 2010).

Here, we focus on the influence of *T*, *P* and chlorine content on the solubility of gold. Although Guo et al. (2018) showed that gold solubility in hydrothermal fluid with low sulfur and high chlorine levels is positively correlated with *T* at 500–800 °C and 2000 bar, the response between Au solubility and *T* in our experiments was not obvious (Fig. 8A), indicating the responses of Au-Cl and Au-S complexes to temperature are different. Williams-Jones et al. (2009) also indicated that the concentration of Au-Cl complexes in the hydrothermal fluid increases significantly with increasing temperature, but Au-S complexes may not increase or even decrease above 500 °C. Loucks and Mavrogenes (1999) found that when the pressure increased from 110 to 400 MPa, the solubility of gold increased significantly, which is consistent with our experimental results (Fig. 8B). The solubility of gold responds weakly to the concentration of chlorine in hydrothermal fluids containing reduced sulfur below 500 °C (Seward, 1973; Hayashi and Ohmoto, 1991; Benning and Seward, 1996). However, Au-Cl complexes may dominate at high *T* and *P* in sulfur-bearing fluids, as demonstrated by Guo et al. (2018), who found the solubility of gold increased with increasing chlorine concentration at 500–800 °C; this is consistent with our experimental results (Fig. 8C).

Note that the only source of Au in our synthetic FIs is the Au capsule, the container of our sample. Therefore, the reported Au solubilities are minimum values because FIs could be formed and isolated from the source before reaching equilibrium. Additionally, note that the S_3^- ion was not detected in our FIs but was indicated from 20 to 250 °C in the in situ Raman spectra of the S-H_2S-CH_4-H_2O system and its subsystems collected from FSCCs (Yu et al., 2021). This is because their samples were under much higher fO_2 conditions than ours, as indicated by the presence of elemental S in their samples under experimental *P*-*T* conditions. Given that Au solubilities in our experiments in reduced H_2S fluids were quite high (up to 3599 ppm) and that S_3^- ions were not detected in our synthetic FIs (Fig. 5), the $Au(HS)S_3^-$ complex, proposed as the most significant Au transporting agent by Pokrovski et al. (2015) under more oxidizing conditions, may not be the only important Au-bearing complex related to the

transport of Au in hydrothermal solutions. The effects of other species, such as Au-polysulfides (AuS_nS^-, n = 2–7), HS_n^- and S_n^{2-}, under various physicochemical conditions need to be further investigated.

5. CONCLUSION

In this study, FSCCs were used for the first time to achieve quantitative loading of H_2S in synthetic FI experiments, and a systematic study of gold solubility in hydrothermal fluids containing H_2S at 600–800 °C and 100–200 MPa was carried out. Our results, which were based on LA-ICP-MS analyses of synthetic FIs, showed that increasing the *P* and sodium chloride concentration increased the solubility of gold. On the other hand, *T* had limited influence. Based on Raman spectroscopy and previous studies, hydrogen sulfide in the gold capsule was partially transformed into S or H_2S_n at high *T*, and HS_n^- and S_n^{2-} formed through deprotonation of H_2S_n may have played considerable roles in the transport of Au in hydrothermal ore-forming processes. The observed enhancement of Au solubility with increasing NaCl concentration indicated the importance of Au-Cl species in chlorine-rich hydrothermal fluids at high *T*s. Therefore, HS_n-Au and Au-Cl may be the two main forms of gold-bearing complexes governing the migration of Au in reduced H_2S-bearing hydrothermal fluids. In addition, the pressure reduction caused by fracturing of rocks may be one of the mechanisms for gold precipitation from magmatic hydrothermal fluids.

DECLARATION OF COMPETING INTEREST

The authors declare that they have no known competing financial interests or personal relationships that could have appeared to influence the work reported in this paper.

ACKNOWLEDGMENTS

We thank Dr. Y. Wan, Ms. Y. Chen and Ms. H.Y. Zhang at the Institute of Deep-sea Science and Engineering (IDSSE), the Chinese Academy of Sciences (CAS), for their assistance in our experiments. Constructive reviews were provided by the Executive Editor (Dr. J. Catalano), Associate Editor (Dr. Z. Zajacz), Guest Editor (Dr. Yuan Mei), two anonymous reviewers, and Dr. Nanfei Cheng of IDSSE, CAS. This work was supported by the National Natural Science Foundation of China (No. 41973059).

APPENDIX A. SUPPLEMENTARY MATERIAL

Supplementary material to this article can be found online at https://doi.org/10.1016/j.gca.2022.03.006.

REFERENCES

Benning L. G. and Seward T. M. (1996) Hydrosulphide complexing of Au (I) in hydrothermal solutions from 150–400 ℃ and 500–1500 bar. *Geochim. Cosmochim. Acta* **60**, 1849–1871.

Berndt M. E., Buttram T., Earley-III D. and Seyfried W. E. (1994) The stability of gold polysulfide complexes in aqueous sulfide solutions: 100 to 150 ℃ and 100 bars. *Geochim. Cosmochim. Acta* **58**, 587–594.

Chou I. M. (1986) Permeability of precious metals to hydrogen at 2 kb total pressure and elevated temperatures. *Am. J. Sci.* **286**, 638–658.

Chou I. M., Song Y. and Burruss R. C. (2008) A new method for synthesizing fluid inclusions in fused silica capillaries containing organic and inorganic material. *Geochim. Cosmochim. Acta* **72**, 5217–5231.

Colin A., Schmidt C., Pokrovski G. S., Wike M., Borisova A. Y. and Toplis M. J. (2020) In situ determination of sulfur speciation and partitioning in aqueous fluid-silicate melt systems. *Geochem. Perspect. Lett.* **14**, 31–35.

Dadze T. P., Kashirtseva G. A. and Ryzhenko B. N. (2000) Gold solubility and species in aqueous sulfide solutions at T = 300 (degree) c. *Geochem. Int.* **38**, 708–712.

Dubessy J., Boiron M. C., Moissette A., Monnin C. and Stretenskaya N. (1992) Determination of water, hydrates and pH in fluid inclusions by micro-Raman spectrometry. *Eur. J. Mineral.* **4**, 885–894.

Duc-Tin Q., Audetat A. and Keppler H. (2007) Solubility of tin in (Cl, F) -bearing aqueous fluids at 700 ℃, 140 MPa: a LA-ICPMS study on synthetic fluid inclusions. *Geochim. Cosmochim. Acta* **71**, 3323–3335.

Emsbo P., Hofstra A. H., Lauha E. A., Griffin G. L. and Hutchinson R. W. (2003) Origin of high-grade gold ore, source of fluid components, and genesis of the Meikle and neighbouring Carlin-type deposits, Northern Carlin Trend, Nevada. *Econ. Geol.* **98**, 1069–1105.

Feneyrol J., Demaiffe D., Ohnenstetter D., Fallick A. E., Dubessy J., Martelat J.-E., Rakotondrazafy A. F. M., Omito E., Ichangi D., Nyamani C. and Wamunyu A. (2017) Age and origin of the tsavorite and tanzanite mineralizing fluids in the Neoproterozoic Mozambique Metamorphic Belt. *Can. Mineral.* **55**, 763–786.

Frezzotti M. L., Tecce F. and Casagli A. (2012) Raman spectroscopy for fluid inclusion analysis. *J. Geochem. Explor.* **112**, 1–20.

Gammons C. H. and Williams-Jones A. E. (1997) The disproportionation of gold (I) chloride complexes at 25 to 200 ℃. *Geochim. Cosmochim. Acta* **61**, 1971–1983.

Gibert F., Pascal M.-L. and Pichavant M. (1998) Gold solubility and speciation in hydrothermal solutions: experimental study of the stability of hydrosulphide complex of gold (AuHS°) at 350 to 450 ℃ and 500 bars. *Geochim. Cosmochim. Acta* **62**, 2931–2947.

Giuliani G., Dubessy J., Banks D., Vinh H. G., Lhomme T., Pironon J., Garnier V., Trinh P. T., Long P. V., Ohnenstetter D. and Schwarz D. (2003) CO_2-H_2S-COS-S_8-AlO(OH)-bearing fluid inclusions in ruby from marble-hosted deposits in Luc Yen area, North Vietnam. *Chem. Geol.* **194**, 167–185.

Guillong M., Meier D., Allan M., Heinrich C. and Yardley B. (2008) Appendix A6: SILLS: a MATLAB-based program for the reduction of laser ablation ICP-MS data of homogeneous materials and inclusions. *Mineral. Assoc. Canada Short Course* **40**, 328–333.

Guo H., Audétat A. and Dolejs D. (2018) Solubility of gold in oxidized, sulfur-bearing fluids at 500–850 ℃ and 200–230 MPa: a synthetic fluid inclusion study. *Geochim. Cosmochim. Acta* **222**, 655–670.

Hayashi K. I. and Ohmoto H. (1991) Solubility of gold in NaCl and H_2S bearing aqueous solutions at 250–350 ℃. *Geochim. Cosmochim. Acta* **55**, 2111–2126.

Heinrich C. A., Guenter D., Audetat A., Ulrich T. and Frischknecht R. (1999) Metal fractionation between magmatic

brine and vapor, determined by microanalysis of fluid inclusions. *Geology* **27**, 755–758.

Hurai V., Cernusak I. and Randive K. (2019) Raman spectroscopic study of polysulfanes (H_2S_n) in natural fluid inclusions. *Chem. Geol.* **508**, 15–29.

Jacquemet N., Guillaume D., Zwick A. and Pokrovski G. S. (2014) In situ Raman spectroscopy identification of the S_3^- ion in S-rich hydrothermal fluids from synthetic fluid inclusions. *Am. Mineral.* **99**, 1109–1118.

Jégo S. and Dasgupta R. (2013) Fluid-present melting of sulfide-bearing ocean-crust: experimental constraints on the transport of sulfur from subducting slab to mantle wedge. *Geochim. Cosmochim. Acta* **110**, 106–134.

Jochum K. P., Weis U., Stoll B., Kuzmin D., Yang Q., Raczek I., Jacob D. E., Stracke A., Birbaum K., Frick D. A., Günther D. and Enzweiler J. (2011) Determination of reference values for NIST SRM 610–617 glasses following ISO guidelines. *Geostand. Geoanal. Res.* **35**, 397–429.

Landtwing M. R., Furrer C., Redmond P. B., Pettke T., Guillong M. and Heinrich C. A. (2010) The Bingham Canyon porphyry Cu-Mo-Au deposit. III. Zoned copper-gold ore deposition by magmatic vapor expansion. *Econ. Geol.* **105**, 91–118.

Li J. L., Schwarzenbach E. M., John T., Ague J. J., Huang F., Gao J., Klemd R., Whitehouse M. J. and Wang X. S. (2020) Uncovering and quantifying the subduction zone sulfur cycle from the slab perspective. *Nat. Commun.* **11**, 514.

Liu X., Sprik M. and Cheng J. (2013) Hydration, acidity and metal complexing of polysulfide species: a first principles molecular dynamics study. *Chem. Phys. Lett.* **563**, 9–14.

Loucks R. R. and Mavrogenes J. A. (1999) Gold solubility in supercritical hydrothermal brines measured in synthetic fluid inclusions. *Science* **284**, 2159–2163.

Mao S. and Duan Z. (2008) The P,V,T,x properties of binary aqueous chloride solutions up to T=573 K and 100 MPa. *J. Chem. Thermodyn.* **40**, 1046–1063.

Matthews W., Linnen R. L. and Guo Q. (2003) A filler-rod technique for controlling redox conditions in cold-seal pressure vessels. *Am. Mineral.* **88**, 701–707.

Migdisov A. A., Suleimenov O. M. and Alekhin Y. V. (1998) Experimental study of polysulfane stability in gaseous hydrogen sulfide. *Geochim. Cosmochim. Acta* **62**, 2627–2635.

Pan P. and Wood S. A. (1991) Gold-chloride complexes in very acidic aqueous solutions and at temperatures 25–300 ℃: a laser Raman spectroscopic study. *Geochim. Cosmochim. Acta* **55**, 2365–2371.

Pokrovski G. S., Tagirov B. R., Schott J., Bazarkina E. F., Hazemann J. L. and Proux O. (2009a) An in situ X-ray absorption spectroscopy study of gold-chloride complexing in hydrothermal fluids. *Chem. Geol.* **259**, 17–29.

Pokrovski G. S., Tagirov B. R., Schott J., Hazemann J. L. and Proux O. (2009b) A new view on gold speciation in sulfur-bearing hydrothermal fluids from in situ X-ray absorption spectroscopy and quantum-chemical modeling. *Geochim. Cosmochim. Acta* **73**, 5406–5427.

Pokrovski G. S. and Dubrovinsky L. S. (2011) The S_3^- ion is stable in geological fluids at elevated temperatures and pressures. *Science* **331**, 1052–1054.

Pokrovski G. S., Akinfiev N. N., Borisova A. Y., Zotov A. V. and Kouzmanov K. (2014) Gold speciation and transport in geological fluids: Insights from experiments and physical-chemical modelling. *Geological Society, London, Special Publications* **402**, 9–70.

Pokrovski G. S. and Dubessy J. (2015) Stability and abundance of the trisulfur radical ion in hydrothermal fluids. *Earth Planet. Sci. Lett.* **411**, 298–309.

Pokrovski G. S., Kokh M. A., Guillaume D., Borisova A. Y., Gisquet P., Hazemann J.-L., Lahera E., Del Net W., Proux O. and Testemale D. (2015) Sulfur radical species form gold deposits on Earth. *PNAS* **112**, 13484–13489.

Pope J. G., Brown K. L. and McConchie D. M. (2005) Gold concentrations in springs at Waiotapu, New Zealand: implications for precious metal deposition in geothermal systems. *Econ. Geol.* **100**, 677–687.

Schmidt C. and Seward T. M. (2017) Raman spectroscopic quantification of sulfur species in aqueous fluids: ratios of relative molar scattering factors of Raman bands of H_2S, HS^-, SO_2, HSO_4^-, SO_4^{2-}, $S_2O_3^{2-}$, S_3^-, and H_2O at ambient conditions and information on changes with pressure and temperature. *Chem. Geol.* **467**, 64–75.

Seo J. H., Guillong M. and Heinrich C. A. (2009) The role of sulfur in the formation of magmatic-hydrothermal copper-gold deposits. *Earth Planet. Sci. Lett.* **282**, 323–328.

Seo J. H., Guillong M. and Heinrich C. A. (2012) Separation of molybdenum and copper in porphyry deposits: the roles of sulfur, redox, and pH in ore mineral deposition at Bingham Canyon. *Econ. Geol.* **107**, 333–356.

Seward T. M. (1973) Thio complexes of gold and the transport of gold in hydrothermal ore solutions. *Geochim. Cosmochim. Acta* **37**, 379–399.

Shenberger D. M. and Barnes H. L. (1989) Solubility of gold in aqueous sulphide solutions from 150 to 350 ℃. *Geochim. Cosmochim. Acta* **53**, 269–278.

Stefánsson A. and Seward T. M. (2003) Stability of chloride gold(I) complexes in aqueous solutions from 300 to 600 ℃ and from 500 to 1800 bar. *Geochim. Cosmochim. Acta* **67**, 4559–4576.

Stefánsson A. and Seward T. M. (2004) Gold(I) complexing in aqueous sulfide solutions to 500 ℃ at 500 bar. *Geochim. Cosmochim. Acta* **68**, 4121–4143.

Sterner S. M. and Bodnar R. J. (1984) Synthetic fluid inclusions in natural quartz. I. Compositional types synthesized and applications to experimental geochemistry. *Geochim. Cosmochim. Acta* **48**, 2659–2668.

Steudel R. and Eckert B. (2003) *Elemental sulfur and sulfur-rich compounds II*. Springer Science & Business Media.

Tagirov B. R., Salvi S., Schott J. and Baranova N. N. (2005) Experimental study of gold-hydrosulphide complexing in aqueous solutions at 350–500 ℃, 500 and 1000 bars using mineral buffers. *Geochim. Cosmochim. Acta* **69**, 2119–2132.

Tomkins A. G. and Evans K. A. (2015) Separate zones of sulfate and sulfide release from subducted mafic oceanic crust. *Earth Planet. Sci. Lett.* **428**, 73–83.

Tritlla J., Alonso-Azcarate J. and Bottrell S. H. (2000) Molten sulphur-dominated fluids in the origin of a native sulphur mineralization in lacustrine evaporites from Cervera del Rio Alhama (Cameros Basin, NE Spain). *J. Geochem. Explor.* **69–70**, 183–187.

Ulrich T., Gunther D. and Heinrich C. A. (2002) The evolution of a porphyry Cu-Au deposit, based on LA-ICP-MS analysis of fluid inclusions: Bajo de la Alumbrera, Argentina. *Econ. Geol.* **97**, 1889–1920.

Wang X., Chou I. M., Hu W. and Burruss R. C. (2013) In situ observations of liquid-liquid phase separation in aqueous $MgSO_4$ solutions: geological and geochemical implications. *Geochim. Cosmochim. Acta* **103**, 1–10.

Wiewiorowski T. K. and Touro F. J. (1966) The sulfur-hydrogen sulfide system. *J. Phys. Chem.* **70**, 234–238.

Williams-Jones A. E. and Heinrich C. A. (2005) Vapour transport and the formation of magmatic-hydrothermal ore deposits. *Econ. Geol.* **100**, 1287–1312.

Williams-Jones A. E., Bowell R. and Migdisov A. A. (2009) Gold in solution. *Elements* **5**, 281–287.

Yu Y., Hu W., Chou I. M., Jiang L., Wan Y., Li Y., Xin Y. and Wang X. (2021) Species of sulfur in sour gas reservoir: insights from in situ Raman spectroscopy of S-H_2S-CH_4-H_2O System and its subsystems from 20 to 250 ℃. *Geofluids* **245**, 1–14.

Zhang L., Audétat A. and Dolejs D. (2012) Solubility of molybdenite (MoS_2) in aqueous fluids at 600–800 ℃, 200 MPa: a synthetic fluid inclusion study. *Geochim. Cosmochim. Acta* **77**, 175–185.

Zajacz Z., Seo J. H., Candela P. A., Piccoli P. M., Heinrich C. A. and Guillong M. (2010) Alkali metals control the release of gold from volatile-rich magmas. *Earth Planet. Sci. Lett.* **297**(1–2), 50–56.

Zajacz Z., Candela P. A. and Piccoli P. M. (2017) The partitioning of Cu, Au and Mo between liquid and vapor at magmatic temperatures and its implications for the genesis of magmatic-hydrothermal ore deposits. *Geochim. Cosmochim. Acta* **207**, 81–101.

Guest editor: Yaun Mei